BIOLOGICAL CRYSTALLOGRAPHY

ISSN 1399-0047

The structure of *Aquifex aeolicus* FtsH in the ADP-bound state reveals a C_2-symmetric hexamer

Marina Vostrukhina,[a] Alexander Popov,[b] Elena Brunstein,[c] Martin A. Lanz,[a,d] Renato Baumgartner,[a] Christoph Bieniossek,[a,e] Magdalena Schacherl[c] and Ulrich Baumann[c]*

[a]Department of Chemistry and Biochemistry, University of Bern, Freiestrasse 3, Bern, CH-3012, Switzerland, [b]European Synchrotron Radiation Facility, 6 Rue Jules Horowitz, Grenoble, F-38043, France, [c]Institute of Biochemistry, University of Cologne, Otto-Fischer-Strasse 12-14, Cologne, D-50674, Germany, [d]Department of Biochemistry, University Walk, University of Bristol, Bristol BS8 1TD, England, and [e]Roche Pharma Research and Early Development, Infectious Diseases Discovery, Roche Innovation Center Basel, F. Hoffmann-La Roche Ltd, Grenzacherstrasse 124, 4070 Basel, Switzerland. *Correspondence e-mail: ubaumann@uni-koeln.de

Received 21 November 2014
Accepted 24 March 2015

Edited by G. J. Kleywegt, EMBL–EBI, Hinxton, England

Keywords: AAA protease; metalloprotease; crystal disorder.

PDB references: *A. aeolicus* FtsH, 4ww0; 4z8x

Supporting information: this article has supporting information at journals.iucr.org/d

The crystal structure of a truncated, soluble quadruple mutant of FtsH from *Aquifex aeolicus* comprising the AAA and protease domains has been determined at 2.96 Å resolution in space group *I*222. The protein crystallizes as a hexamer, with the protease domain forming layers in the *ab* plane. Contacts between these layers are mediated by the AAA domains. These are highly disordered in one crystal form, but are clearly visible in a related form with a shorter *c* axis. Here, adenosine diphosphate (ADP) is bound to each subunit and the AAA ring exhibits twofold symmetry. The arrangement is different from the ADP-bound state of an analogously truncated, soluble FtsH construct from *Thermotoga maritima*. The pore is completely closed and the phenylalanine residues in the pore line a contiguous path. The protease hexamer is very similar to those described for other FtsH structures. To resolve certain open issues regarding a conserved glycine in the linker between the AAA and protease domains, as well as the active-site switch β-strand, mutations have been introduced in the full-length membrane-bound protein. Activity analysis of these point mutants reveals the crucial importance of these residues for proteolytic activity and is in accord with previous interpretation of the active-site switch and the importance of the linker glycine residue.

1. Introduction

The defining feature of the AAA+ family (**A**TPases **a**ssociated with various cellular **a**ctivities) is a conserved ATPase module that forms hexameric or heptameric ring-like structures (Hanson & Whiteheart, 2005; White & Lauring, 2007). AAA+ ATPases are involved in a wide variety of essential cellular processes, for example vesicle transport, organelle assembly, membrane dynamics and protein degradation. Malfunctioning of AAA+ proteases frequently leads to severe pathophysiological conditions. Examples are inclusion-body myopathy associated with Paget's disease of the bone and frontotemporal dementia (IBMPFD; Ju & Weihl, 2010), Zellweger spectrum diseases (Steinberg *et al.*, 2006) and some forms of hereditary spastic paraplegia (Rugarli & Langer, 2006). Responsible for the latter is a defect in paraplegin, a mitochondrial membrane-bound ATP-dependent metalloprotease that shares about 60% sequence identity with the *Escherichia coli* AAA protease FtsH.

FtsH homologues are universally conserved in eubacteria, mitochondria and chloroplasts, where they are involved in essential processes of intracellular protein degradation, akin to other energy-dependent proteolytic assemblies (Akiyama,

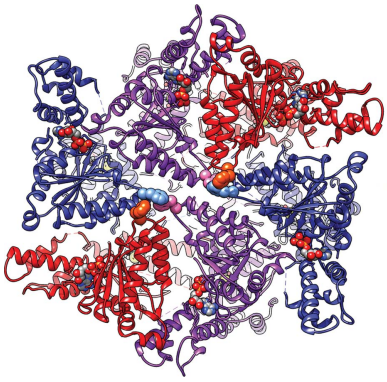

2009; Langklotz *et al.*, 2012; Okuno & Ogura, 2013). FtsH degrades membrane-bound substrates, such as the isolated SecY subunit of the SecYEG translocon or the a subunit of F_o ATPase, and also soluble proteins such as bacteriophage λ-encoded transcription activator CII, the heat-shock sigma factor σ32 and LpxC deacetylase, a key regulator of membrane lipopolysaccharides in *E. coli* (Akiyama, 2009; Langklotz *et al.*, 2012). More recently, further substrates have been identified (Narberhaus *et al.*, 2009; Westphal *et al.*, 2012).

FtsH belongs to the classical clade of the extended AAA group of the AAA+ family (Snider *et al.*, 2008). Contrary to most other ATP-dependent proteases, it contains both AAA and protease domains in the same polypeptide chain. Like other AAA+ proteins, FtsH forms hexameric rings and this oligomeric state is essential for ATPase and proteolytic activity. The bacterial genes encode polypeptide chains of about 600 amino acids in length. They usually contain two N-terminal transmembrane helices separated by an approximately 80-residue periplasmic region, followed by the cytosolic part harbouring the AAA and proteolytic domains. The ATPase module contains the typical nucleotide-binding Walker A and B motifs, as well as the second region of homology (SRH), which displays conserved arginine residues ('arginine fingers') that are thought to be responsible for oligomerization and nucleotide hydrolysis. The ring-like assembly features a narrow central pore, which is characterized by a conserved aromatic residue Φ in the so-called pore motif ΦVG.

Substrates can be recognized either by specific adaptor proteins or directly by the aromatic pore residues (Schlieker *et al.*, 2004; Yamada-Inagawa *et al.*, 2003); in an ATP-dependent mechanism, substrates are unfolded and translocated to the internal degradation compartment through the central narrow pore, which can only admit unfolded substrates (Sauer & Baker, 2011). The current most favoured mechanism describing ATP-dependent unfolding and translocation is the 'pulling model' (Sauer & Baker, 2011; Striebel *et al.*, 2009). Here, the aromatic pore residues grab the substrate and pull it towards the narrow entrance pore, utilizing a mechanical force that is generated by ATP-hydrolysis-triggered conformational rearrangements within the AAA+ module. This leads to unfolding and subsequent translocation of the substrate polypeptide chain, followed by peptide-bond hydrolysis at the active centres in the interior of the assembly. The nature of the conformational changes that transform the chemical energy of the phosphoanhydride bonds into a mechanical force is still obscure owing to a lack of high-resolution crystal structures. However, it is clear that ATP hydrolysis in one subunit triggers a conformational change that is transmitted to one or more neighbouring subunits. The mode of ATP hydrolysis by the six subunits has not yet been conclusively elucidated. Principally, there are three possibilities: a concerted hydrolysis event occurring simultaneously in all subunits, an ordered progression from one subunit to another or a stochastic mechanism in which ATP hydrolysis of each subunit occurs independently of events in the other protomers. Experiments with covalently linked ClpX variant subunits (Martin *et al.*, 2005) and on the Yta10/Yta12 mitochondrial mAAA protease (Augustin *et al.*, 2009) hint at an ordered orchestration of ATP hydrolysis by the different subunits that is possibly accompanied by some stochastic component, while a concerted mechanism appears to be very unlikely. This is also consistent with the observation that frequently not all of the six subunits can be saturated with ATP (Hersch *et al.*, 2005).

For FtsH, the most complete currently available crystal structures comprise the whole cytosolic regions of the enzymes from *Thermotoga maritima* (Δ-*Tm*FtsH) at 2.44 Å resolution (Bieniossek *et al.*, 2006) and from *Thermus thermophilus* (Δ-*Tt*FtsH) at 3.9 Å resolution (Suno *et al.*, 2006, 2012). Both show a homohexameric architecture built by two separate rings that are formed by the AAA and protease domains, respectively. While the protease ring exhibits virtually perfect sixfold symmetry in both structures, the AAA rings in the *T. maritima* and *T. thermophilus* structures are very different; they show C_2 and C_3 symmetry, respectively, although both structures have six ADP molecules bound to the AAA moieties. In addition, the completely nucleotide-free structure of the cytosolic region of the *T. maritima* protein (apo Δ-*Tm*FtsH) has been reported at 2.60 Å resolution, showing perfect sixfold symmetry for both rings and revealing an active-site switch segment in the protease domain that forms a β-strand for binding the substrate in an extended conformation (Bieniossek *et al.*, 2009).

The two ADP-bound structures led to different conclusions on the conformational rearrangements within the AAA+ ring during the ATPase cycle and on the putative substrate-translocation mechanism, as well as different interpretations of the active-site switch segment in the protease domain.

In order to gain more structural insight into the mechanism of substrate translocation, we report here a third ADP-bound crystal structure, namely that of the cytosolic region of FtsH comprising residues 142–634 from the hyperthermophilic organism *Aquifex aeolicus* (Δ-*Aa*FtsH). For a more complete understanding of the effects of point mutations in the context of the full-length protein, we have also expressed the complete FtsH protein from *A. aeolicus*, including the N-terminal transmembrane helices and the periplasmic domain (FL-*Aa*FtsH). Our new structure, together with our previous results and additional biochemical data, favours our earlier conclusions on the conformational rearrangements and the movement of the aromatic pore residues, as well as the role of the active-site switch segment (Bieniossek *et al.*, 2006, 2009).

2. Materials and methods

2.1. Cloning, protein expression and purification of soluble FtsH constructs

The cytosolic region of *A. aeolicus* FtsH (amino acids 142–634) was amplified by polymerase chain reaction (PCR) from *A. aeolicus* genomic DNA using the primers 5′-GTGGTATTCCATATGGCGAAGGTTTACATAGAGG-3′ and 5′-CTTCCGCTCGAGTCAGACTACCTCCTCCTTAACTTC-3′, and cloned into pET-28a expression vector (Merck Millipore)

with an N-terminal thrombin-cleavable hexahistidine tag using the NdeI and XhoI restriction sites (underlined). The construct has four mutations, I250M, F360L, K552R and E627G, that were unintentionally introduced by the PCR and cloning procedure. Protein expression was performed in *E. coli* BL21 (DE3) CodonPlus cells (Agilent Technologies) as described below. Selenomethionine-labelled protein was prepared as described by Van Duyne *et al.* (1993).

A gene encoding FtsH (amino acids 126–624) from *T. thermophilus* bearing the G399L mutation [Δ-*Tt*FtsH(G399L)] was synthesized employing codon-usage optimization for *E. coli* (MrGene, Regensburg, Germany) and subcloned into pET-22b expression vector (Merck Millipore) with a C-terminal hexahistidine tag using NdeI and HindIII restriction sites. For protein expression, the plasmid was transformed into *E. coli* BL21 (DE3) Rosetta cells (Merck Millipore).

For all of these soluble constructs, protein expression was induced with 1 m*M* isopropyl *β*-D-1-thiogalactopyranoside (IPTG) at an optical density (OD_{600}) of 0.8–1.0 and cell growth continued overnight at 22°C. The cells were then harvested by centrifugation, washed twice with lysis buffer (20 m*M* Tris–HCl, 300 m*M* NaCl, 0.02% NaN_3 pH 8.0), resuspended in 10 ml lysis buffer per gram of cells and frozen at −20°C. The cells were disrupted by three passages through a French press at 6.9 MPa. Ethylenediaminetetraacetic acid (EDTA)-free cOmplete protease-inhibitor cocktail tablets (Roche) or, alternatively, 0.2 m*M* phenylmethanesulfonyl-fluoride (PMSF) was added. The lysate was cleared by centrifugation (20 000*g*) and the supernatant was passed over a nickel–nitrilotriacetic acid (Ni–NTA) column (Qiagen) followed by Resource Q anion-exchange chromatography (GE Healthcare) and size-exclusion chromatography as described previously (Bieniossek *et al.*, 2006).

For Δ-*Aa*FtsH, the purification protocol was modified by cleaving the N-terminal His tag with thrombin overnight at 4°C followed by another step of Ni–NTA chromatography. Fractions were concentrated and loaded onto a Superdex S200 16/600 gel-filtration column (GE Healthcare) equilibrated with 20 m*M* Tris–HCl pH 8.0, 100 m*M* NaCl, 0.02% NaN_3. The elution fractions were analyzed by dynamic light scattering (DynaPro, Protein Solutions).

2.2. Cloning, expression and purification of full-length FtsH

The gene coding for full-length *A. aeolicus* FtsH (FL-*Aa*FtsH) was amplified by PCR from the genomic DNA using the primers 5′-GGGAATTCCATATGAACGCGTTGAAA-AACTTC-3′ and 5′-CCGCTCGAGGACTACCTCCTCCTT-AACTTCTTCAG-3′. The resulting PCR product was digested and ligated into the NdeI and XhoI sites of pET-22a. The resulting plasmid was transformed into *E. coli* strain C43. Cultures were grown in lysogeny broth (LB) medium supplemented with ampicillin (100 μg l^{-1}) at 37°C to an OD_{600} of 0.7. Expression was induced by adding 1 m*M* IPTG and continued at 30°C for 5 h. Cells were disrupted in a cell disruptor (Constant Systems, UK) and membranes were isolated by ultracentrifugation at 250 000*g* after clearing cell debris at 24 000*g*. The membranes were resuspended in 0.1 *M* Tris pH 7.5, 100 m*M* NaCl, 1% dodecylmaltoside (DDM) for 4 h at 4°C. The extract was diluted 1:1 with a buffer consisting of 300 m*M* NaCl, 10 m*M* imidazole pH 7.5 and cleared at 250 000*g*. The supernatant was again diluted 1:1 as above and loaded onto an Ni–NTA column (Qiagen) equilibrated with 20 m*M* Tris pH 7.5, 300 m*M* NaCl, 10 m*M* imidazole, 0.03% DDM, followed by washing with buffer containing 60 m*M* imidazole. Bound protein was finally eluted with 250 m*M* imidazole. FtsH fractions were pooled, concentrated and loaded onto a HiLoad 16/600 Superdex gel-filtration column equilibrated with a buffer consisting of 20 m*M* Tris pH 7.5, 100 m*M* NaCl, 5% glycerol, 0.03% DDM.

2.3. Crystallization, data collection, structure solution and refinement

Crystals of soluble Δ-*Aa*FtsH were obtained using protein solution at 10–30 mg ml^{-1} in vapour-diffusion experiments at 18°C with either 2 *M* ammonium sulfate, 0.1 *M* Tris–HCl pH 8.5, 10 m*M* EDTA or, as another condition, 60% Tacsimate pH 7.0, 10 m*M* adenylyl imidodiphosphate lithium salt hydrate (AMP-PNP). One crystal form grew in both conditions. It belonged to space group *I*222, with unit-cell parameters a = 127.8, b = 188.4, c = 206.2 Å. Dehydration experiments were essential to obtain useful diffraction data from this first crystal form. For this, the reservoir concentration was changed to 3 *M* ammonium sulfate and the crystals were equilibrated overnight.

Some months after harvesting crystals from the Tacsimate condition, much smaller crystals of another crystal form were observed in the same drop. They also belonged to space group *I*222, but with different unit-cell parameters: a = 138.2, b = 162.3, c = 170.2 Å.

Diffraction data were measured at 110 K in-house (Rigaku MSC, RU300 rotating copper anode; R-AXIS IV image plate) and on beamlines X06SA (Pilatus 6M detector) and X06DA (PXIII, MAR225 CCD) at the Swiss Light Source (SLS), Paul Scherrer Institute, Villigen, Switzerland and on beamline ID23.1 at the European Synchrotron Radiation Facility (ESRF), Grenoble, France, the latter being equipped with an ADSC Q315R CCD detector. The data-collection strategy was generated with *MOSFLM* (Battye *et al.*, 2011) at the SLS and with *MOSFLM* and *BEST* (Bourenkov & Popov, 2010) at the ESRF. In particular, *BEST* proved to be essential for collecting complete data sets owing to the pronounced radiation-sensitivity and weak diffraction properties of the crystals. Data were integrated and scaled with *XDS* (Kabsch, 2010). For molecular replacement, *Phaser* was used (McCoy *et al.*, 2007). The protease domain from *A. aeolicus* FtsH (PDB entry 2di4; Suno *et al.*, 2006) and the ATPase domain from *T. maritima* FtsH (PDB entry 2ce7; 65% sequence identity; Bieniossek *et al.*, 2006) were used as search models. Model building was performed in the *Crystallographic Object-Oriented Toolkit* (*Coot*; Emsley *et al.*, 2010). Refinement was carried out with *PHENIX* (Adams *et al.*, 2011; Afonine *et al.*,

2012) using rigid-body refinement followed by individual site, ADP and TLS refinement. For the selenomethionine anomalous peak data, the heavy-atom positions were determined by *SHELXD* (Sheldrick, 2010) and *phenix.hyss* (Zwart *et al.*, 2008). Phases were computed using *SHARP* (Bricogne *et al.*, 2003). Further density modification, phase extension, automatic model building and refinement were performed with *PHENIX*. Later, *BUSTER* (Blanc *et al.*, 2004; Smart *et al.*, 2012) was used for the final refinement steps. Figures were created with *Chimera* (Pettersen *et al.*, 2004) and *PyMOL* (http://www.pymol.org).

2.4. Activity assays

ATPase activity measurements were performed using the EnzChek Phosphate Assay Kit (Invitrogen) in 96-well plates (Greiner) using a Biotek Synergy H4 plate reader. Reaction buffer [5 µl, 20×; 1 *M* Tris–HCl pH 7.5, 20 m*M* $MgCl_2$, 2 m*M* NaN_3, 20 µl 1 m*M* 2-amino-6-mercapto-7-methylpurine riboside substrate solution (MESG) and 3 µl purine nucleoside phosphorylase (3 units)] and purified FtsH protein were mixed in a total volume of 100 µl. The mixture was incubated for 10 min at room temperature. Adenosine triphosphate (ATP; 2 m*M*) was added and the change in absorbance at 360 nm was recorded using a plate reader (Synergy H4, Biotek).

The protease activity of the purified FtsH proteins was determined using resorufin-labelled casein (Roche) as a substrate. Resorufin-labelled casein substrate solution [25 µl, 0.4%(*w*/*v*)], incubation buffer (25 µl; 0.2 *M* Tris–HCl pH 7.8, 2 m*M* ATP, 0.02 *M* $CaCl_2$) and sample solution (50 µl; 0.1 mg protein in gel-filtration buffer) were incubated at 60°C. Reactions were terminated after 0, 15, 30, 60 and 120 min by adding 240 µl 5%(*w*/*v*) trichloroacetic acid and further incubation at 37°C for 15 min. Samples were centrifuged at 12 000*g* for 5 min before 200 µl of supernatant was mixed with 600 µl assay buffer (0.5 *M* Tris–HCl pH 8.8). Protease activity was determined by measuring the absorbance at 574 nm.

3. Results

3.1. A crystal form of soluble Δ-*Aa*FtsH with lattice packing mediated by disordered AAA domains

In this study, we used a truncated FtsH construct from *A. aeolicus* (UniProt O67077) spanning residues 142–634, which thus lacks the N-terminal transmembrane helices and the periplasmic domain (Δ-*Aa*FtsH; Supplementary Fig. S1). Sequencing of this construct revealed four point mutations: I250M, F360L, K552R and E627G. In other FtsH proteins from different species, Ile250 is substituted by leucine and Lys552 by arginine and leucine. Glu627 is sometimes replaced by threonine and lysine, and is located in the nonconserved C-terminal extension, which is disordered in our crystal structure. Phe360 is more conserved but, for example, it is replaced by a leucine in the mitochondrial FtsH homologue iAAA protease/Yme1 from yeast (UniProt P32795). The residue is located within a loop in the small α-helical subdomain of the AAA part, where it contributes to hydrophobic interactions within this subdomain. It is within the neighbourhood of the ATP-binding cleft but makes no contacts to the nucleotide. Its *in silico* replacement by leucine appears not to disturb the structure and, as discussed below, the mutant still binds nucleotides.

Expression yielded large amounts of protein, about 60–100 mg per litre of culture, indicating a stably folded polypeptide chain. The protein was purified to homogeneity by Ni–NTA and size-exclusion chromatography, where it eluted as a monomer. The truncated and mutated protein was inactive in ATPase and proteolytic assays. This is in contradiction to an

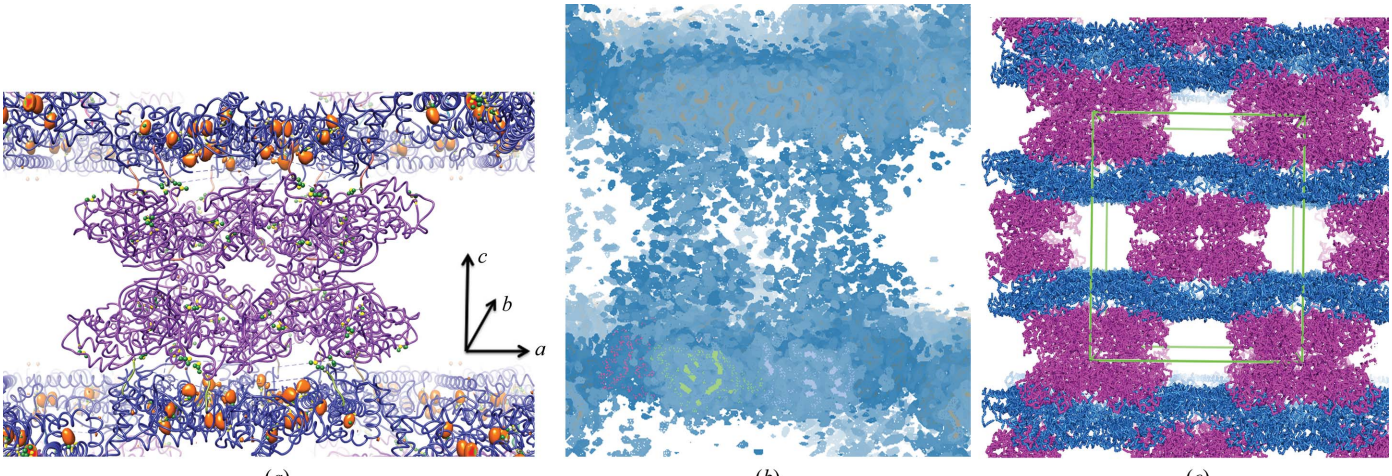

(*a*) (*b*) (*c*)

Figure 1
Evidence for disordered AAA domains in crystal form X1. (*a*) An imaginary Fourier map calculated from selenomethionine peak data is contoured at 4σ above the mean. Overlaid is a model consisting of the molecular-replacement solution of the protease domains (blue ribbon) with a very approximate model of the position of the AAA domains (magenta). The positions of the methionine side chains are indicated by ball-and-stick side chains; selenium is shown in yellow. (*b*) The experimental solvent-modified electron-density map calculated from SAD phases contoured at 1σ of the region displayed in (*a*) together with a C^{α} trace of the protease domains. (*c*) Crystal lattice in the second crystal form with ordered AAA domains. The AAA domains are shown in magenta and the protease domains in blue. The unit cell is drawn in green with the *c* axis running vertically and the *a* axis horizontally.

Table 1
Data-collection and refinement statistics.

Values in parentheses are for the outermost shell. Values in square brackets refer to refinement with the AAA domains omitted.

Data set	Δ-*Aa*FtsH-X1, native	Δ-*Aa*FtsH-X1, SeMet	Δ-*Aa*FtsH-X2
PDB entry	4z8x	—	4ww0
Data collection			
X-ray source	X06SA, SLS	X06SA, SLS	ID23.1, ESRF
Detector	Pilatus 6M	Pilatus 6M	ADSC Q315R CCD
Space group	*I*222	*I*222	*I*222
a, *b*, *c* (Å)	127.8, 188.4, 206.2	128.7, 188.6, 208.2	138.2, 162.3, 170.2
Wavelength (Å)	1.0000	0.9795	0.97930
Resolution (Å)	100.0–3.25 (3.33–3.25)	100.0–3.39 (3.48–3.39)	79.7–2.96 (3.03–2.96)
Multiplicity	3.7 (3.8)	3.9 (3.8)†	5.3 (4.2)
Completeness (%)	99.3 (96.4)	99.5 (95.5)	97.9 (91.3)
R_{merge}‡	0.045 (1.25)	0.069 (0.760)	0.089 (1.37)
$CC_{1/2}$	1.0 (0.64)	1.0 (0.83)	1.0 (0.43)
$\langle I/\sigma(I)\rangle$	18.6 (1.4)	11.8 (1.6)	14.0 (1.0)
Wilson *B* factor (Å^2)	132.2	116.8	86.7
Refinement statistics			
Resolution range (Å)	43.22–3.25		43.01–2.96
No. of unique reflections	39311		39476
No. of test reflections	2005		1972
R_{work}/R_{free}	0.226/0.253 [0.242/0.263]		0.209/0.248
No. of protein non-H atoms	10035 [4185]		9891
No. of water molecules	[3]		3
No. of ions/heavy atoms	[3]		3
No. of other atoms	69 [10]		84
No. of TLS groups	9 [3]		6
Root-mean-square deviations from ideal values§			
Bond lengths (Å)	0.010		0.009
Bond angles (°)	1.11		1.12
Average *B* factor (Å^2)			
Overall	222.0		112.0
All protein atoms	221.8		112.3
Protease/AAA domain	141.0/283.1		94.8/125.0
Water	132.0		85.7
Other atoms	140.1		138.7
MolProbity statistics¶			
Ramachandran favoured/disallowed	90.9/1.8 [94.7/1.0]		93.9/1.9
Rotamer outliers (%)	8.4 [7.7]		5.7
Clashscore	6.4 [5.5]		6.0

† Friedel pairs are counted as separate reflections. ‡ $R_{merge} = \sum_{hkl}\sum_i |I_i(hkl) - \langle I(hkl)\rangle| / \sum_{hkl}\sum_i I_i(hkl)$, where $I_i(hkl)$ is the *i*th measurement of the intensity of the unique reflection *hkl* and $\langle I(hkl)\rangle$ is the mean over all symmetry-related measurements. § Standard geometries taken from Engh & Huber (2001) as implemented in *BUSTER*. ¶ *MolProbity* scores (Chen *et al.*, 2010) as implemented in *PHENIX*.

earlier report in which the protease domain alone of FtsH from *A. aeolicus* was described to be hexameric and proteolytically active (Suno *et al.*, 2006); this discrepancy could possibly be explained by the four point mutations, although it does not appear to be very likely.

Large crystals of Δ-*Aa*FtsH were initially obtained under ammonium sulfate conditions but only diffracted to about 5 Å resolution and were difficult to cryoprotect. These crystals could be improved by the addition of EDTA and by dehydration to a diffraction limit of about 3.25 Å resolution (Table 1). While all three protease monomers in the asymmetric unit were easily localized using the deposited coordinates of this domain (PDB entry 2di4; Suno *et al.*, 2006) and *Phaser* (McCoy *et al.*, 2007), further structure solution of this crystal form was hampered by a lack of success in placing the AAA domains. Similarly, a selenomethionine single-wavelength anomalous diffraction (SAD) experiment with the same crystal form easily allowed the location of 12 Se atoms (out of 36, including the N-terminal methionine), all of which are situated within the protease domains. None of those present in the AAA moieties could be found (Fig. 1*a*) either by employing Patterson/direct methods or by anomalous difference Fourier synthesis using phases derived from the protease domain. A solvent-flattened electron-density map calculated from these 12 Se-atom positions was very well defined for the protease domains, but the density for the AAA moieties was weak (Fig. 1*b*). Eventually, two AAA domains could be placed with some confidence and a third could be placed at a reasonable position in the electron-density maps. Refinement using *BUSTER-TNT* (Smart *et al.*, 2012) with and without inclusion of the AAA part converged with similar R/R_{free} values of 0.232/0.258 and 0.238/0.264, respectively (Table 1). Difference electron-density maps indicated the possible presence of a nucleotide in one of the subunits, but this is difficult to confirm owing to the weak electron density. The refined ADP factors of the AAA moieties are about twice those obtained for the protease domains. In summary, the AAA domains in this crystal form have very weak electron density and are mainly disordered, but nevertheless mediate crystal contacts in the *c* direction. These crystal contacts are weaker than those formed by the protease domains and this is also visible in the anisotropic diffraction by these crystals, where the anisotropic *B* tensor differs by 86 Å^2 between the *b** and *c** directions.

The largely disordered AAA domains of the Δ-*Aa*FtsH structure in this crystal form together with the solvent region leaves only about 15% of the volume of the asymmetric unit well ordered and this poses problems for the proper definition of a bulk-solvent mask. Furthermore, for many randomly chosen test sets the R_{free} was lower than the R_{work} after several rounds of refinement with *BUSTER*. Picking the test reflections in small spheres in reciprocal space using *DATAMAN* (Kleywegt & Jones, 1996) in order to avoid coupling of test and work set by the large 'solvent' region *via* the Rossmann *G*-function cured this problem.

The same crystal form was also obtained from 60% Tacsimate pH 7.0 in the presence of the nonhydrolysable ATP analogue AMP-PNP at 10 m*M*. Some time after harvesting

crystals from this condition, smaller crystals of a different shape appeared in those drops side by side with the original crystals. It is possible that the harvesting process created new nucleation centres or that proteolytic events took place that gave rise to this new crystal form. These crystals also belonged to space group *I*222, with three monomers in the asymmetric unit, but differ in their unit-cell parameters (Table 1). In particular, the *c* axis is considerably shortened, leading to a stronger contact between the AAA domains. Data were collected on beamline ID23.1 at the ESRF, Grenoble, France and the structure was solved shortly after data collection by molecular replacement, including the positions of all three AAA domains in the asymmetric unit. In the following, the results of the analysis of this crystal form will be described.

3.2. Overall structure

In both crystal forms, the crystallographic twofold axis in the *c* direction creates the hexameric ring from the three independent protease monomers. This assembly is virtually identical to those observed in the other Δ-FtsH crystal structures, including the hexameric and proteolytically active *T. maritima* ADP-bound Δ-*Tm*FtsH (PDB entries 2cea and 2ce7; Bieniossek *et al.*, 2006) and the structure of the *A. aeolicus* proteolytic domain (PDB entry 2di4; Suno *et al.*, 2006). The flat protease rings form extended zigzag layers in the *ab* plane (Fig. 1*c*). Contacts between these layers are mediated by the AAA domains of two hexamers that interact in a head-to-head fashion, thus forming a dodecameric superassembly in the crystal lattice. This dodecamer is clearly a crystallization artifact as inferred by the opposite orientation of the two hexamers with respect to a membrane that would be on the side of the AAA moieties. Nevertheless, dodecamer formation from two hexamers buries 12 670 Å^2 of a total of 209 090 Å^2 of accessible surface, as calculated by *CNS* (Brunger, 2007). The assembly is judged to be stable by the *PISA* server (Krissinel & Henrick, 2007). Thus, these crystal contacts between the AAA domains are strong, especially when compared with the other Δ-FtsH crystal structures from *T. maritima* and *T. thermophilus*, in which the major contacts are formed by back-to-back packing of the protease rings and the interactions between the AAA domains are much weaker in those crystal forms.

The final Δ-*Aa*FtsH model contains the three crystallographically independent FtsH monomers spanning residues 142–607. Amino acids at the termini or flexible loops are disordered and are therefore omitted from the model. Data-collection and refinement statistics are given in Table 1.

As in the other FtsH structures of the cytosolic region, the architecture of the hexameric particle consists of two rings, one formed by the protease domains and the other by the AAA moieties (Fig. 2).

3.3. The protease ring is sixfold symmetric and identical to all other FtsH structures

The protease ring has exact sixfold symmetry (Fig. 2*c*) and is, as mentioned above, virtually identical to those observed in the similarly truncated constructs of FtsH from *T. thermophilus* (Suno *et al.*, 2006) and *T. maritima* (Bieniossek *et al.*, 2006, 2009) and the isolated *A. aeolicus* protease domain (Suno *et al.*, 2006). This is noteworthy because these proteins are reported to occur in solution as functional hexamers, while the truncated Δ-*Aa*FtsH elutes as a monomer from a gel-filtration column. Apparently, spontaneous reassembly takes place under crystallization conditions with high protein concentrations. The stability of the protease homohexameric plate is provided by the large interface between the two adjacent subunits, burying about 2500 Å^2 of surface between adjacent subunits. Thus, the protease ring appears to be a robust structural entity that is not likely to be influenced by any conformational changes of the AAA+ domains.

The monomer of the protease ring consists of the six α-helices α10–α15, with the long helix α13 building the base of

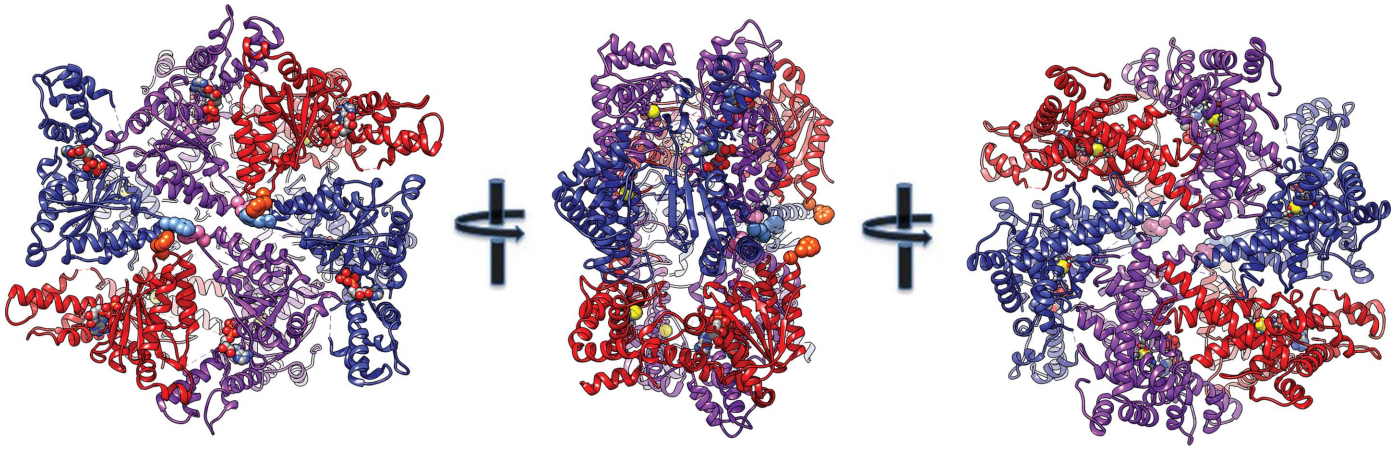

Figure 2
The hexameric structure of Δ-*Aa*FtsH in crystal form X2. The molecule is shown in three different views related by an approximate 90° rotation around the vertical. ADP is shown as a ball-and-stick model and Zn^{2+} as grey spheres. The pore residue Phe228 is shown in representation with large spheres. Monomers related by the crystallographic twofold axis have the same colour (subunit *A*, red; subunit *B*, blue; subunit *C*, violet). (*a*) View of the AAA ring. (*b*) Side view. (*c*) View of the protease ring.

the protease ring. There are two short β-strands, β7 and β8 (Fig. 3 and Supplementary Fig. S1).

FtsH belongs to an aspzincin family owing to the characteristics of its active site, in which an aspartic acid (Asp496)

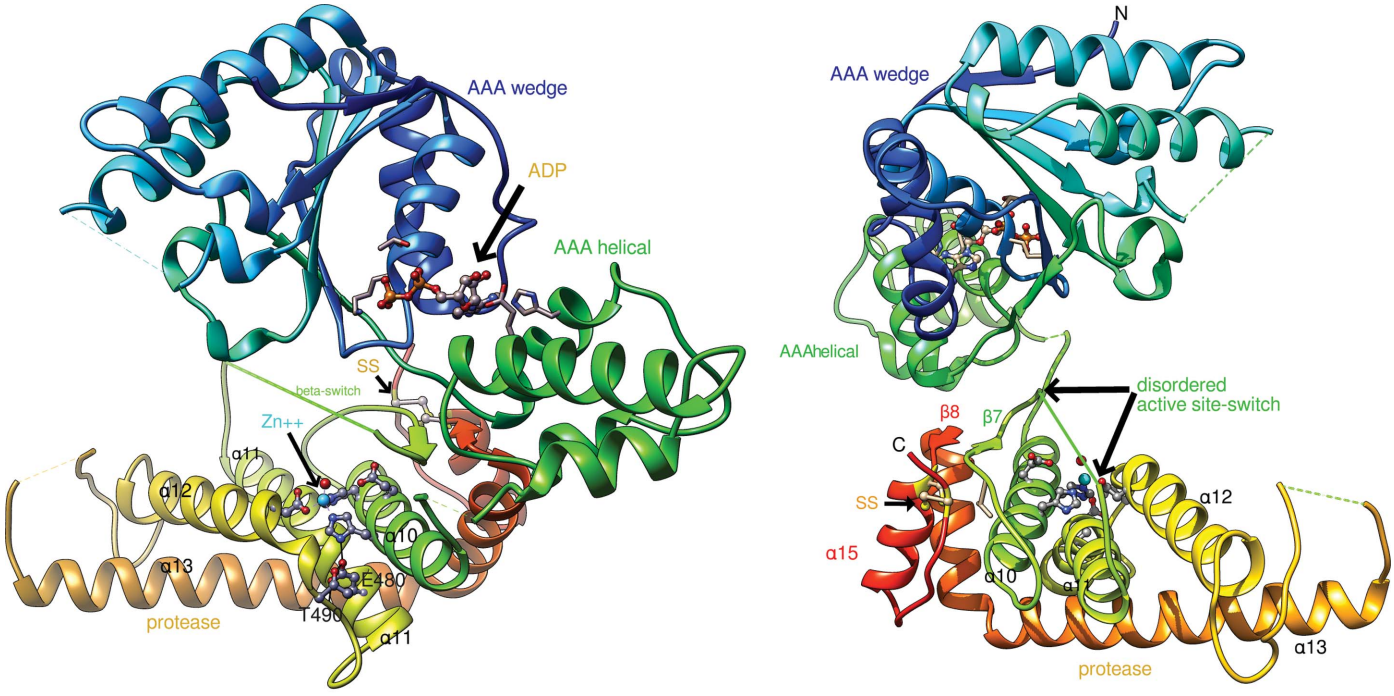

Figure 3
The FtsH monomer structure. Two views of the monomer rotated by about 180° around the vertical axis are shown. The rainbow colouring runs from blue (N-terminus) to red (C-terminus). The active-site zinc ion and its coordinating water molecule are depicted as cyan and red spheres, respectively. In the protease moiety, the zinc ligands (His418, His422 and Asp496), as well as the catalytic base (Glu419) and residues Glu480 and Thr490, are depicted in a ball-and-stick representation (O atoms in red, N atoms in blue). Some (secondary) structure elements that are referred to in the text are also labelled. In the AAA domain, which is composed of the 'wedge' and helical subdomains, bound ADP is shown together with residues Lys201 and Thr202 from the Walker A motif, as well as His338 and Glu366.

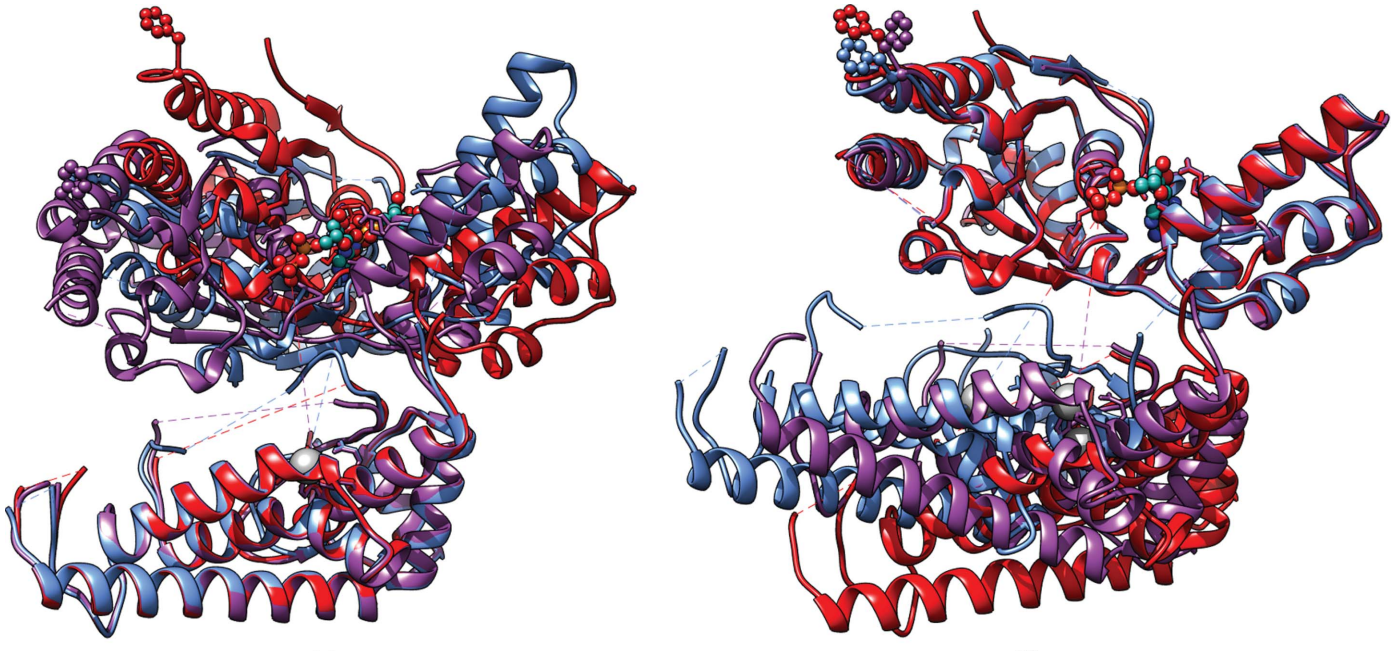

Figure 4
Overlay of the three crystallographically independent monomers. An overlay using the protease domain (*a*) or the AAA domain (*b*) as a reference is shown. The colouring of the subunits is as in Fig. 2. Phe228 and ADP are shown as ball-and-stick models, as well as the active-site Zn^{2+}. The huge rigid-body domain motions are visible, as well as the lack of changes within the AAA moiety itself.

functions as a zinc ligand. The catalytic site of the protease domain is located at a rather peripheral position of the hexamer plate in a cleft between helices α10 and α12. Helix α10 carries the characteristic metalloprotease active-site fingerprint ^{418}HE*XX*H^{422}, with the two histidine residues acting as zinc ligands and the glutamic acid as the catalytic base.

The zinc ion is pyramidally coordinated by the two N$^{\varepsilon 2}$ atoms of the histidine side chains and the *syn* lone pair of O$^{\delta 2}$ of residue Asp496, which is located in helix α12. The fourth coordination site has been interpreted as a water molecule, although the density at this position in some subunits appears to be stronger and may hint at a carboxylic acid from the crystallization buffer. In the third independent molecule (subunit *C*) there is the suggestion of an alternative conformation of His422 accompanied by some Zn^{2+} depletion, probably caused by the additive EDTA.

Helix α12 bears the ^{490}(T/S)(T/S)GA*X*(N/D)D^{496} motif with Asp496 as the third zinc ligand. The first side-chain hydroxyl group of this sequence motif forms a hydrogen bond to Glu480, which in turn hydrogen-bonds to the first zinc ligand His418, thus fixing it in the conformation required for zinc coordination (Fig. 3*a*). Helix α11 forms the bottom of the cleft formed by helices α10 and α12 and runs roughly antiparallel to these. Just beyond the pyramidal base formed by the three zinc ligands His418, His422 and Asp496, it undergoes

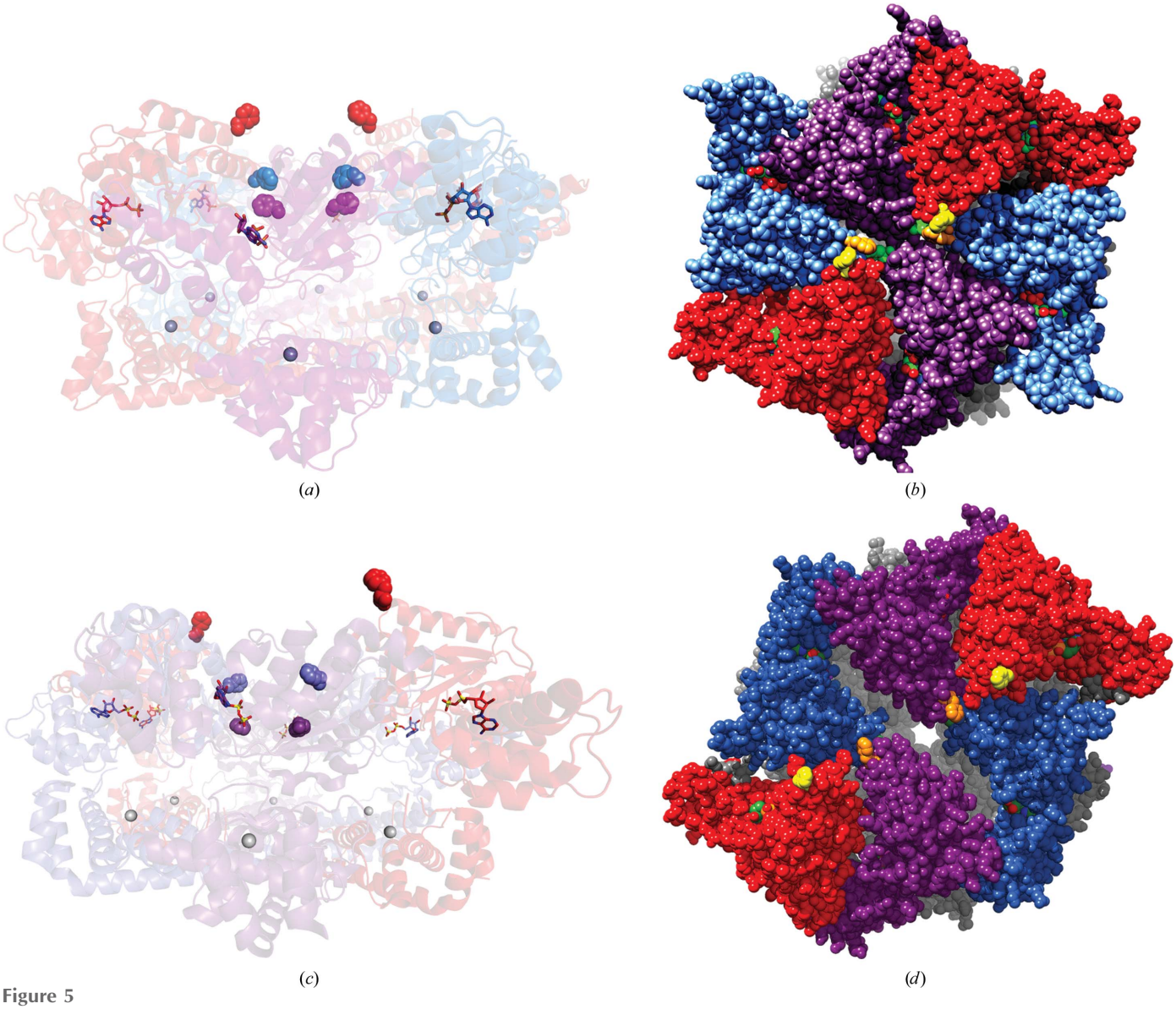

Figure 5
Approximate positions of the aromatic pore residues. (*a*) Side view of Δ-*Aa*FtsH with bound ADP shown as a transparent cartoon. Phe228 is shown with large spheres. Also depicted are ADP and the catalytic zinc ion. (*b*) Space-filling representation of Δ-*Aa*FtsH with Phe228 being represented as slightly larger spheres shown in yellow, orange and green. The AAA domains are colour-coded as in Fig. 2, *i.e.* subunit *A* in red (Phe228 yellow), subunit *B* in blue (Phe228 orange) and subunit *C* in violet (Phe228 in green). The protease domains are shown in grey. ADP is depicted with green C atoms. (*c*, *d*) Similar representations of Δ-*Tm*FtsH in the ADP-bound state (PDB entry 2ce7). The pore phenylalanine residues (Phe234) are also coloured yellow, orange and green, although the latter is not visible here because it is buried in the interior.

a sharp bend of about 40° introduced by the two glycine residues of the conserved ^{475}GGR*XX*EE^{481} motif.

At the C-terminus there is a disulfide bond formed between Cys588 and Cys606 that appears to be unique to *A. aeolicus* FtsH. It is also found in the crystal structure of the isolated protease domain of FtsH from *A. aeolicus* (Suno *et al.*, 2006). It is unclear whether this S–S bridge is formed within the cytosol, *i.e.* under native conditions, although it might contribute to the thermostability required for *A. aeolicus* proteins. However, the covalent bonds between the cysteines appear to be formed to a lesser extent in crystal form X1, hinting at the possibility that they formed during prolonged exposure to air in the crystallization droplet.

3.4. The AAA ring possesses C_2 symmetry and is different from Δ-*Tm*FtsH

The AAA domains assemble into a ring with C_2 symmetry (Fig. 2*a*). The breakdown of the sixfold symmetry in the protease ring to the twofold symmetry of the whole hexamer arises from the different interdomain angles between the protease and AAA domains in the three crystallographically independent monomers (Fig. 4). The domains move as rigid bodies by a rotation of some 30°, as analyzed by the *DynDom* server (Lee *et al.*, 2003), with the hinge region located approximately at residues 400–410, *i.e.* within the linker connecting the AAA and protease domains. In the hexameric particle, monomers in opposition to each other possess the same interdomain angle but differ from the other two pairs, thus reducing the symmetry from C_6 in the protease ring to C_2 in the AAA ring. This is principally very similar to Δ-*Tm*FtsH in the ADP-bound state. However, there is a qualitative difference in the AAA domain motions between the Δ-*Tm*FtsH and Δ-*Aa*FtsH structures: while the rotations in Δ-*Tm*FtsH occur around an axis mainly perpendicular to that connecting the centres of the two domains, *i.e.* perpendicular to the plane of the protease ring (closure, as defined by the *DynDom* server, of >70%), in Δ-*Aa*FtsH the rotations possess a more lateral (twisting) component. The closure amounts here to only 36% for chains *B* and *C*, 73% for chains *A* and *B*, and 98% for chains *A* and *C*. Thus, the path on which the AAA domains move from one conformation (as specified by the change in interdomain angle) to another has a larger component parallel to the protease ring in Δ-*Aa*FtsH compared with Δ-*Tm*FtsH. Consequently, the arrangement of the AAA domains in the AAA rings of the Δ-*Tm*FtsH and Δ-*Aa*FtsH structures is very different, although both possess C_2 symmetry. While the protease rings align very well, none of the AAA domains superpose between the two structures when the protease ring is taken as a reference.

The AAA domains move as rigid bodies and there is no additional change in the angle between the so-called 'wedge' and 'helical' subdomains. This is expected since all of the AAA domains have ADP bound (Fig. 4) and the nucleotide influences the intradomain angle in AAA ATPases.

As a result, very different shapes of the substrate-entrance clefts and different spatial arrangements of the pore residues ^{228}FGV are observed in Δ-*Aa*FtsH and Δ-*Tm*FtsH (Fig. 5). The pore phenylalanine residues are partially disordered, but their approximate positions could be defined from the neighbouring residues. Compared with the Δ-*Tm*FtsH structure, the crucial aromatic side chains of the pore motif ^{228}FGV are more buried inside the cleft and line a more contiguous, funnel-shaped path. There is also a much closer contact in the Δ-*Aa*FtsH structure compared with Δ-*Tm*FtsH between the nucleotide-binding site of subunit *C* and the arginine-finger motif (residues 313–316) of subunit *A*.

Three ADP molecules were identified in the electron-density maps, each bound to one protomer (Fig. 6). ADP is a contaminant of AMP-PNP preparations and appears to have a higher affinity. It binds to the AAA module in the cleft between the so-called wedge and helical subdomains (Fig. 3). The phosphate O atoms are coordinated by the Walker A motif *via* residues Gly198 (backbone NH), Gly200 (backbone NH), Lys201 (backbone NH and side-chain N$^{\zeta}$), Thr202 (backbone NH and side-chain O$^{\gamma1}$) and Leu203 (backbone NH) (Supplementary Fig. S1, Fig. 6). The ribose 3′-OH group forms a hydrogen bond to the side chain of Glu366. The N3 atom of the adenine base is hydrogen-bonded to the side chain of His338, and Ala158 forms a hydrogen bond with its main-chain NH and carbonyl O atom to N6 and the N1 extra-ring amino group, respectively.

3.5. Inhibition of β-strand formation in the active-site switch inactivates FtsH

Previous analysis of the Δ-*Tm*FtsH apo structure (PDB entry 3kds) revealed the presence of an active-site switch in the form of the segment comprising residues 452–458 in the *T. maritima* apoenzyme (Bieniossek *et al.*, 2009). In the ADP-bound Δ-*Tm*FtsH crystal form, this segment is disordered in five NCS-related copies and adopts an α-helical conformation in the remaining subunit (Bieniossek *et al.*, 2006). However, in all three NCS-related copies of the apo structure of Δ-*Tm*FtsH it forms an additional β-strand running parallel to and just above the active-site helix α10, providing a binding site for the main chain of the substrate. This β-strand complements the two-stranded β-ribbon that is present in all FtsH structures by adding an additional antiparallel strand just above the active-site helix α10 (Fig. 3 and

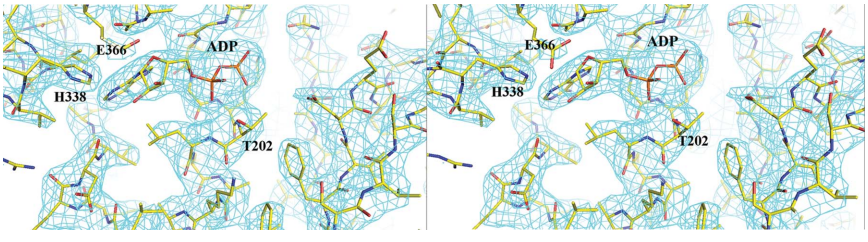

Figure 6
$2F_o - F_c$ density map at the ADP-binding site. The map is contoured at 0.11 e Å^{-3} (1.05 r.m.s.) and is shown in magenta together with the refined model.

Supplementary Fig. S1). In metzincins, a clan of very distantly related metalloproteases, the corresponding segment has the same function and was termed the 'edge strand' (Cerdà-Costa & Gomis-Rüth, 2014; Gomis-Rüth, 2003). A substrate-mimetic inhibitor bound to the apo Δ-*Tm*FtsH structure confirms the function of this additional, obviously conformationally mobile β-strand. In the Δ-*Aa*FtsH ADP-bound structure reported here, a larger segment spanning residues 447–456, including this active-site switch, is disordered in all three crystallographically independent copies.

A different interpretation of this segment has been given for the structure of a soluble Δ-*Tt*FtsH construct. Here, an α-helical structure, termed the 'lid-helix', was described, which switches between a straight and a kinked conformation at residue Gly448 in the open and closed conformation, respectively, thereby sequestering the proteolytic active site in the latter state (Suno *et al.*, 2006, 2012). One problem with this interpretation is the lack of a substrate-binding structural element in the protease domain. As mentioned above, even distantly related metalloproteases possess a β-sheet covering the active-site α-helix, where the outmost β-strand (called the 'edge strand') serves as an edge to which the substrate polypepide chain can dock as an additional β-strand, presenting the scissile peptide bond to the catalytic machinery and the zinc-bound water. A second problem with the lid-helix point of view arises from analysis of the electron density of this element in the Δ-*Tt*FtsH structure: OMIT maps clearly show that this segment is also disordered in the Δ-*Tt*FtsH structure (Supplementary Fig. S2). Presumably, the lid-helix interpretation is owing to the strong model bias present in the density maps of the Δ-*Tt*FtsH structure owing to the very low resolution (3.9 Å) and the likely use of the square root of the structure-factor amplitudes ($F^{1/2}$) in the refinement instead of the structure-factor amplitudes (F) or intensities ($I = |F|^2$), as explained in the Supporting Information.

To further investigate the role of this additional antiparallel β-strand in the activity of FtsH, we have introduced the T450P mutation in this segment within the full-length FtsH protein from *A. aeolicus* (FL-*Aa*FtsH) including both transmembrane helices and periplasmic region and bearing no other mutations anywhere; *i.e.* the four point mutations in the soluble construct Δ-*Aa*FtsH used for crystallization are not present in all of the full-length constructs discussed here. The T450P mutation should impede the formation of a regular β-strand. Indeed, the proteolytic activity of the mutant turned out to be severely affected (Fig. 7), but most of its ATPase activity was retained.

3.6. A conserved glycine in the linker between AAA and the protease domain is functionally important

The structure of the cytoplasmic part of FtsH from *T. thermophilus* (Δ-*Tt*FtsH) was determined at 3.9 Å resolution. To improve the crystal quality to this resolution, an absolutely conserved glycine residue (Gly399 in *T. thermophilus* and *A. aeolicus* FtsH) in the linker region between the protease and ATPase domains was mutated to leucine (Suno *et al.*, 2006, 2012). The mutant was reported to behave like the wild type. As reported previously, we introduced the same mutation in the *T. maritima* construct Δ-*Tm*FtsH(G404L) and found that this mutant elutes exclusively as a monomer from a Superdex S200 gel-filtration column and is inactive in ATPase and proteolytic assays (Bieniossek *et al.*, 2009).

We repeated this experiment for the truncated *T. thermophilus* FtsH (residues 126–624) by introducing the same G399L mutation [Δ-*Tt*FtsH(G399L)]. This truncated and mutated protein is virtually inactive in both the proteolytic and ATPase assays (Fig. 7). It possesses about 6% of the proteolytic activity compared with FL-*Aa*FtsH and about 10% of the proteolytic activity compared with Δ-*Tt*FtsH. In order to test the importance of this glycine linker in the context of the full-length protein, we introduced the same mutation into full-length *Aa*FtsH [FL-*Aa*FtsH (G399L)]. This mutated protein is expressed at much lower levels than the wild-type protein and possesses only about 5% of the wild-type proteolytic activity, but it retains some 40% of the wild-type FL-*Aa*FtsH ATPase activity.

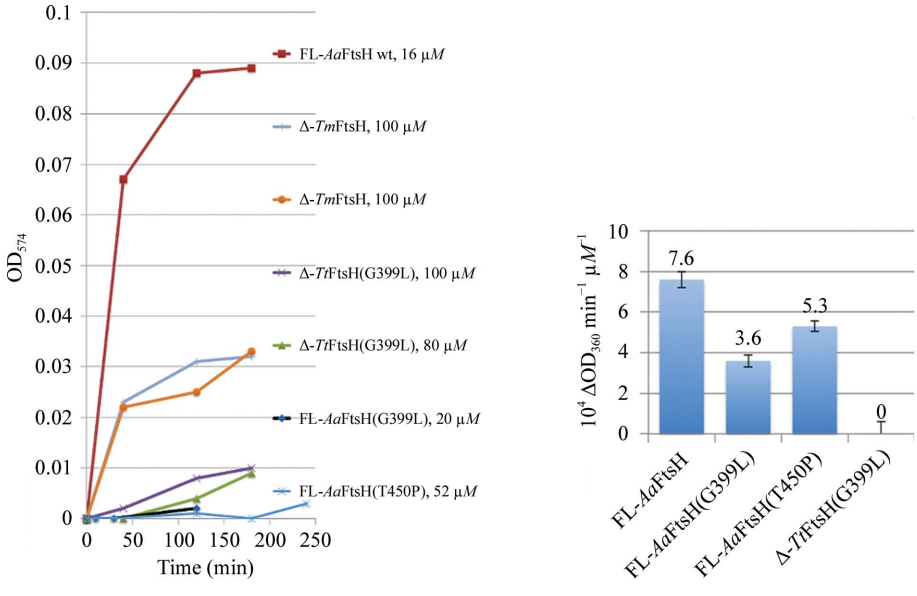

Figure 7
Activity assays of FtsH mutants. Left, resorufin–casein proteolytic assay time course. Proteolytic activity is given as absorbance change over time (min) at 574 nm. From top to bottom: background-corrected data for wild-type full-length FL-*Aa*FtsH (16 µ*M*; red line), wild-type Δ-*Tm*FtsH (double experiment at 100 µ*M*; light blue and orange lines), Δ-*Tt*FtsH (100 and 80 µ*M*; lilac and green lines), FL-*Aa*FtsH(G399L) (20 µ*M*; black line) and FL-*Aa*FtsH(T450P) (52 µ*M*; blue line). Right, ATPase activities given as absorbance change $\times 10^4$ at 360 nm per minute and per micromole of protein for, from left to right, wild-type FL-*Aa*FtsH, FL-*Aa*FtsH(G399L), FL-*Aa*FtsH(T450P) and truncated Δ-*Tt*FtsH(G399L).

Thus, we conclude that this glycine in the linker region between the AAA and protease domains is crucial for FtsH activity, which is in agreement with its strict conservation in all FtsH proteins from all species.

4. Discussion

We have determined the crystal structure of a truncated FtsH construct from *A. aeolicus* spanning the AAA and protease domains. The protein, although a monomer in solution, crystallizes as a hexamer with a sixfold-symmetric protease ring virtually identical to all of the other FtsH structures reported to date.

The AAA domains in the crystal forms described here are involved in crystal contacts between layers formed by the protease domains. Despite this, in one crystal form the AAA domains are disordered and exhibit only very fragmented electron density. After several months and possible concomitant dehydration, a new crystal form with a shrunken unit cell was observed. In this crystal form all of the AAA domains are ordered and have ADP bound. Similar to the previously reported structure of Δ-*Tm*FtsH, the AAA ring possesses twofold symmetry. However, the detailed conformations of the AAA rings are very different between *A. aeolicus* FtsH and *T. maritima* FtsH. In the Δ-*Aa*FtsH structure the packing is tighter in the plane of the AAA ring, leading to a much narrower pore compared with the Δ-*Tm*FtsH structure. Considering the fact that the AAA domains are heavily involved in crystal lattice contacts, the situation in solution may be different. Nevertheless, it shows the range of motions that are accessible to the AAA ring. The *A. aeolicus* and *T. maritima* FtsH proteins exhibit 48% sequence identity over the full length and, if taken separately, the protease and AAA domains of these two structures in the ADP-bound state show almost perfect overlay, with a root-mean-square deviation (r.m.s.d.) of about 0.7 Å. No intradomain movement of the AAA domain is observed in both structures, in agreement with the fact that all of the subunits have ADP bound.

The protease assemblies of all published FtsH structures are very similar to each other. In the ADP-bound Δ-*Tm*FtsH structure the active-site switch β-strand is mostly disordered or α-helical, as noted in the publication on the apo Δ-*Tm*FtsH structure (Bieniossek *et al.*, 2009). In the Δ-*Aa*FtsH structure reported here this segment is invisible in all three independent copies. In the Δ-*Tt*FtsH structure its role has been interpreted as a 'lid-helix' (Suno *et al.*, 2006, 2012). This view is problematic because without this active-site switch β-strand there is no obvious binding site for the substrate peptide, a hitherto unknown observation for other proteolytic enzymes. Beside this, there are crystallographic issues regarding the Δ-*Tt*FtsH structure. As we show in the Supporting Information, the model has most likely been refined against systematically flawed data (Supplementary Table S1), probably arising from the mislabelling of the amplitudes as intensities. In any case, it should be emphasized that this structure was determined at a resolution of only 3.9 Å and that the relevant segment is virtually entirely disordered in the electron-density maps (Supplementary Fig. S2). Mutations in this segment introducing proline residues inactivate FtsH as described by Suno *et al.* (2012) and as demonstrated in our study presented here.

In summary, we have determined a crystal structure of the cytosolic region of FtsH in the ADP-bound state with a new arrangement of the AAA moieties, shedding light on the conformational space that can be sampled by rigid-body movements. The high flexibility of the AAA domains is also highlighted by their disorder in one crystal form.

5. Related literature

The following references are cited in the Supporting Information for this article: Gouet *et al.* (2003), Murshudov *et al.* (1997) and Padilla & Yeates (2003).

Acknowledgements

This work was supported by the University of Bern (Switzerland), the Swiss National Science Foundation (grants 3100A0-108262 and 31003A-120174) and the University of Cologne. Data-collection experiments were performed on the ID23.1 beamline at the European Synchrotron Radiation Facility (ESRF), Grenoble, France and the X06SA and X06DA beamlines at the Swiss Light Source (SLS), Paul Scherrer Institute, Villigen. We are grateful for all of the support received at these beamlines, and especially to Dr Meitian Wang and Dr Clemens Schulze-Briese at SLS. We thank Dr Isabel Uson, CSIC Barcelona, Spain and Dr Piotr Neumann, University Göttingen, Germany for essential hints and help in interpreting the disordered AAA domains.

References

Adams, P. D. *et al.* (2011). *Methods*, **55**, 94–106.
Afonine, P. V., Grosse-Kunstleve, R. W., Echols, N., Headd, J. J., Moriarty, N. W., Mustyakimov, M., Terwilliger, T. C., Urzhumtsev, A., Zwart, P. H. & Adams, P. D. (2012). *Acta Cryst.* D**68**, 352–367.
Akiyama, Y. (2009). *J. Biochem.* **146**, 449–454.
Augustin, S., Gerdes, F., Lee, S., Tsai, F. T., Langer, T. & Tatsuta, T. (2009). *Mol. Cell*, **35**, 574–585.
Battye, T. G. G., Kontogiannis, L., Johnson, O., Powell, H. R. & Leslie, A. G. W. (2011). *Acta Cryst.* D**67**, 271–281.
Bieniossek, C., Niederhauser, B. & Baumann, U. M. (2009). *Proc. Natl Acad. Sci. USA*, **106**, 21579–21584.
Bieniossek, C., Schalch, T., Bumann, M., Meister, M., Meier, R. & Baumann, U. (2006). *Proc. Natl Acad. Sci. USA*, **103**, 3066–3071.
Blanc, E., Roversi, P., Vonrhein, C., Flensburg, C., Lea, S. M. & Bricogne, G. (2004). *Acta Cryst.* D**60**, 2210–2221.
Bourenkov, G. P. & Popov, A. N. (2010). *Acta Cryst.* D**66**, 409–419.
Bricogne, G., Vonrhein, C., Flensburg, C., Schiltz, M. & Paciorek, W. (2003). *Acta Cryst.* D**59**, 2023–2030.
Brunger, A. T. (2007). *Nature Protoc.* **2**, 2728–2733.
Cerdà-Costa, N. & Gomis-Rüth, F. X. (2014). *Protein Sci.* **23**, 123–144.
Chen, V. B., Arendall, W. B., Headd, J. J., Keedy, D. A., Immormino, R. M., Kapral, G. J., Murray, L. W., Richardson, J. S. & Richardson, D. C. (2010). *Acta Cryst.* D**66**, 12–21.
Emsley, P., Lohkamp, B., Scott, W. G. & Cowtan, K. (2010). *Acta Cryst.* D**66**, 486–501.
Engh, R. A. & Huber, R. (2001). *International Tables for Crystallography*, Vol. *F*, edited by E. Arnold & M. G. Rossmann, pp. 382–392. Dordrecht: Kluwer Academic Publishers.
Gomis-Rüth, F. X. (2003). *Mol. Biotechnol.* **24**, 157–202.

Gouet, P., Robert, X. & Courcelle, E. (2003). *Nucleic Acids Res.* **31**, 3320–3323.
Hanson, P. I. & Whiteheart, S. W. (2005). *Nature Rev. Mol. Cell Biol.* **6**, 519–529.
Hersch, G. L., Burton, R. E., Bolon, D. N., Baker, T. A. & Sauer, R. T. (2005). *Cell*, **121**, 1017–1027.
Ju, J.-S. & Weihl, C. C. (2010). *Hum. Mol. Genet.* **19**, R38–R45.
Kabsch, W. (2010). *Acta Cryst.* D**66**, 125–132.
Kleywegt, G. J. & Jones, T. A. (1996). *Acta Cryst.* D**52**, 826–828.
Krissinel, E. & Henrick, K. (2007). *J. Mol. Biol.* **372**, 774–797.
Langklotz, S., Baumann, U. & Narberhaus, F. (2012). *Biochim. Biophys. Acta*, **1823**, 40–48.
Lee, R. A., Razaz, M. & Hayward, S. (2003). *Bioinformatics*, **19**, 1290–1291.
Martin, A., Baker, T. A. & Sauer, R. T. (2005). *Nature (London)*, **437**, 1115–1120.
McCoy, A. J., Grosse-Kunstleve, R. W., Adams, P. D., Winn, M. D., Storoni, L. C. & Read, R. J. (2007). *J. Appl. Cryst.* **40**, 658–674.
Murshudov, G. N., Vagin, A. A. & Dodson, E. J. (1997). *Acta Cryst.* D**53**, 240–255.
Narberhaus, F., Obrist, M., Führer, F. & Langklotz, S. (2009). *Res. Microbiol.* **160**, 652–659.
Okuno, T. & Ogura, T. (2013). *Subcell. Biochem.* **66**, 53–69.
Padilla, J. E. & Yeates, T. O. (2003). *Acta Cryst.* D**59**, 1124–1130.
Pettersen, E. F., Goddard, T. D., Huang, C. C., Couch, G. S., Greenblatt, D. M., Meng, E. C. & Ferrin, T. E. (2004). *J. Comput. Chem.* **25**, 1605–1612.
Rugarli, E. I. & Langer, T. (2006). *Trends Mol. Med.* **12**, 262–269.
Sauer, R. T. & Baker, T. A. (2011). *Annu. Rev. Biochem.* **80**, 587–612.
Schlieker, C., Weibezahn, J., Patzelt, H., Tessarz, P., Strub, C., Zeth, K., Erbse, A., Schneider-Mergener, J., Chin, J. W., Schultz, P. G., Bukau, B. & Mogk, A. (2004). *Nature Struct. Mol. Biol.* **11**, 607–615.
Sheldrick, G. M. (2010). *Acta Cryst.* D**66**, 479–485.
Smart, O. S., Womack, T. O., Flensburg, C., Keller, P., Paciorek, W., Sharff, A., Vonrhein, C. & Bricogne, G. (2012). *Acta Cryst.* D**68**, 368–380.
Snider, J., Thibault, G. & Houry, W. A. (2008). *Genome Biol.* **9**, 216.
Steinberg, S. J., Dodt, G., Raymond, G. V., Braverman, N. E., Moser, A. B. & Moser, H. W. (2006). *Biochim. Biophys. Acta*, **1763**, 1733–1748.
Striebel, F., Kress, W. & Weber-Ban, E. (2009). *Curr. Opin. Struct. Biol.* **19**, 209–217.
Suno, R., Niwa, H., Tsuchiya, D., Zhang, X., Yoshida, M. & Morikawa, K. (2006). *Mol. Cell*, **22**, 575–585.
Suno, R., Shimoyama, M., Abe, A., Shimamura, T., Shimodate, N., Watanabe, Y. H., Akiyama, Y. & Yoshida, M. (2012). *FEBS Lett.* **586**, 3117–3121.
Van Duyne, G. D., Standaert, R. F., Karplus, P. A., Schreiber, S. L. & Clardy, J. (1993). *J. Mol. Biol.* **229**, 105–124.
Westphal, K., Langklotz, S., Thomanek, N. & Narberhaus, F. (2012). *J. Biol. Chem.* **287**, 42962–42971.
White, S. R. & Lauring, B. (2007). *Traffic*, **8**, 1657–1667.
Yamada-Inagawa, T., Okuno, T., Karata, K., Yamanaka, K. & Ogura, T. (2003). *J. Biol. Chem.* **278**, 50182–50187.
Zwart, P. H., Afonine, P. V., Grosse-Kunstleve, R. W., Hung, L.-W., Ioerger, T. R., McCoy, A. J., McKee, E., Moriarty, N. W., Read, R. J., Sacchettini, J. C., Sauter, N. K., Storoni, L. C., Terwilliger, T. C. & Adams, P. D. (2008). *Methods Mol. Biol.* **426**, 419–435.